Indonesian Journal of Physics
Vol. 34. No.1, 09 November 2023

Investigation of hydraulic jump by using the Moving Particle Semi-Implicit method

Y Yulianto[1*]
[1]*Physics Department, Halu Oleo University, Jl. H.E.A. Mokodompit, Kendari, 93232, Indonesia*

(Received: 28 September 2023, Revised: 09 November 2023, Accepted: 09 November 2023)

Abstract

Investigation of hydraulic jump is necessary to provide the required data in hydraulic structures. Simulations are an alternative to experiments for providing data. The objective of this modeling is to examine the impact of the reservoir level on the height after the jump and the distance of the jump from the front of the exhaust hole. The simulation was performed by using the Moving Particle Semi-Implicit method. The reservoir level was set to 10 m, 18 m, and 32 m with 18174, 23934, and 33942 particles of simulation, respectively. The obtained results indicate that the height of the reservoir after the jump is between 2.68 m and 3.60 m for an initial reservoir level of 10 m. For an initial reservoir level of 18 m, the height of the jump is between 2.90 and 5.18 m. The final height after the jump ranges from 2.98 m to 8.28 meters for an initial reservoir level of 32 m. Consistent with the findings of other researchers, the simulation outcomes are extremely favorable. The higher the reservoir level, the higher the height after the jump, according to the obtained results of this study. In addition, the distance of the jump from the front of the exhaust hole increases as the reservoir fills. Regarding the expansion of this study, additional research must be conducted to investigate this phenomenon in greater depth, particularly with regard to particle velocity during the hydraulic jump process.

Keywords: hydraulic jump, mesh-less, MPS, reservoir.

INTRODUCTION

Hydraulic jumps hold significant relevance within several engineering and environmental domains, encompassing the development of spillways for dams, hydraulic structures, and water treatment facilities. Fig. 1 shows the model of hydraulic jump. Hydraulic jumps are a subject of research for engineers and scientists who seek to comprehend their characteristics and enhance their efficacy in several applications, including flood control and erosion prevention. The parameters of a hydraulic jump are contingent upon several elements, including the velocity of the flow, the channel shape, and the fluid properties.

Several studies have demonstrated beneficial outcomes in the investigation of hydraulic jumps. The experimental work done by Laishram et al. aimed to investigate the hydraulic jump characteristics in an open channel flume and assess the influence of slope on these features [1]. The utilization of Smoothed Particle Hydrodynamics (SPH) in hydraulic structures is evident in the research conducted by López et al. In their study, they provide an analysis of surface profiles to evaluate the evolution of hydraulic jumps [2]. The internal flow field and associated phenomena during the developmental stage of forced hydraulic jumps were investigated by Cheng et al [3]. In their work, Bonn et al. conducted an investigation on hydraulic jumps characterized by mostly unidirectional flow where these hydraulic jumps were generated by two methods: by limiting the flow within a small channel with parallel walls, or by adding an inflow in the form of a narrow sheet [4].

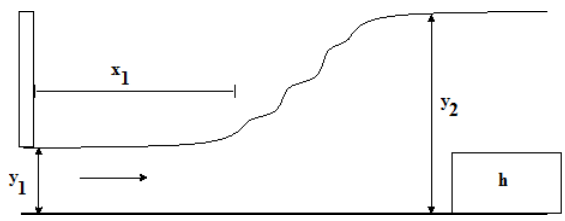

Fig. 1. Diagrammatic depiction of the hydraulic jump.

*Corresponding author.
E-mail address: pramutadi@itb.ac.id

In this study, the simulation was performed by using the Moving Particle Semi-Implicit (MPS) method. The MPS method is a computational methodology, introduced first by Koshizuka and Oka [5]–[8], employed in the field of fluid dynamics and particle-based simulations with the purpose of representing the dynamics of fluids and their interactions with solid entities. The utilization of this technique is prevalent in the realm of fluid flow simulations. The MPS method has been successfully employed in explaining several liquid phenomena, such as stratification process [9]–[12], relocation process [13]–[15], and eutectic case [16], [17].

The objective of this study is to examine the impact of the initial height of the reservoir on the subsequent height seen during the hydraulic leap phenomena. The obtained results derived from this investigation were compared with the results acquired in the study conducted by López et al. [2]. The project aims to generate data that can offer valuable insights into the fluid properties of hydraulic structures.

THEORY

Commonly used for describing incompressible flow is the Navier-Stokes equation, which can be written as [5]–[8]

$$\frac{D\rho}{Dt} = 0 \tag{1}$$

$$\frac{D\vec{u}}{Dt} = -\frac{1}{\rho}\nabla P + v\nabla^2\vec{u} + \vec{g} \tag{2}$$

where $\vec{g}$ is gravity, $\vec{u}$ is velocity vector, v is the kinematic viscosity, P is the pressure, t is the time, ρ is the density, and ∇ is the gradient.

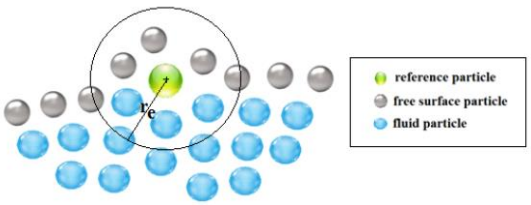

Fig. 2. Free surface boundary condition in MPS framework.

The MPS method is a mesh-less particle technique for analyzing incompressible flow. Particle interactions are defined relative to the reference particle position. It is possible to calculate the motion of a particle based on their interaction using a weight function proportional to distance and the interaction force between the two nearest particles. The formula for the frequently used weight function of the MPS method is as follows

$$w(r) = \begin{cases} \left(1 - \frac{r}{r_e}\right)^2 & 0 \le r \le r_e \\ 0 & r_e \le r \end{cases} \tag{3}$$

where r is the distance between two particles and r_e is the radius of minimal interaction [5]–[8]. As illustrated in Fig. 2, the weight function approaches zero when the distance between two particles is greater than the cut-off radius [5]–[8]. On *i*-particle position, the particle number density, which equates the density of the liquid, can be expressed as

$$n_i = \sum_{j \neq i} w\left(\left|\vec{r}_j - \vec{r}_i\right|\right) \tag{4}$$

where r_i and r_j are the representative of the position vectors of i and j particles [5]–[8]. Using these formulas, the gradient, divergence, and Laplacian models can be calculated

$$\langle\vec{\nabla}\phi\rangle_i = \frac{d}{n^0}\sum_{j \neq i}\frac{\phi_j - \hat{\phi}_i}{\left|\vec{r}_j - \vec{r}_i\right|^2} w\left(\left|\vec{r}_j - \vec{r}_i\right|\right) \tag{5}$$

$$\langle\vec{\nabla}.\vec{\varphi}\rangle_i = \frac{d}{n^0}\sum_{j \neq i}\frac{\varphi_j - \varphi_i}{\left|\vec{r}_j - \vec{r}_i\right|^2}\left(\vec{r}_j - \vec{r}_i\right) w\left(\left|\vec{r}_j - \vec{r}_i\right|\right) \tag{6}$$

$$\langle\nabla^2\phi\rangle_i = \frac{2d}{\lambda n^0}\sum_{j \neq i}\left(\phi_j - \phi_i\right) w\left(\left|\vec{r}_j - \vec{r}_i\right|\right) \tag{7}$$

where d represents the number of spatial dimensions, n^0 represents the initial particle number density, ϕ_i represents the scalar of the j-particle at $\vec{r}_j$, $\hat{\phi}_i$ is the minimum value of the scalar quantity in the effective radius of the i-target particle, and λ is the parameter chosen to make the obtained Laplacian model to be proportional to the analytical solution [5]–[8]. The value of λ can be approximated by

$$\lambda = \frac{\sum_{j \neq i} w\left(\left|\vec{r}_j - \vec{r}_i\right|\right)\left|\vec{r}_j - \vec{r}_i\right|^2}{\sum_{j \neq i} w\left(\left|\vec{r}_j - \vec{r}_i\right|\right)} \cong \frac{\int_V w(r) r^2 dV}{\int_V w(r) dV} \tag{8}$$

To maintain incompressible conditions, the particle number density is kept constant for internal particles while it decreases for particles located on the free surface. The observed particles, considered to be free surface particles as depicted in Fig. 2, must satisfy the condition of

$$n_i < \beta n^0 \tag{9}$$

where β is the constant value which satisfies $\beta < 1$ [5]–[8]. In this study, viscosity term was first implicitly calculated by using the discretized Laplacian model

$$\vec{u}_k^* = \vec{u}_i^k + \nu\Delta t \frac{2d}{\lambda n^0}\sum_{j\neq i}(\vec{u}_j^* - \vec{u}_i^*)w(|\vec{u}_j^k - \vec{u}_i^k|) \quad (10)$$

where the superscript $*$ and k are the representative of the temporary values and the values at the last time step, respectively. Furthermore, new temporal velocity and its corresponding position can be obtained by [5]–[8]

$$\vec{u}^{k+1} = \vec{u}^{**} + \Delta t\left(-\frac{1}{\rho^0}\nabla P\right) \quad (11)$$

$$\vec{r}^{k+1} = \vec{r}^{**} + (\Delta t)^2\left(-\frac{1}{\rho^0}\nabla P\right) \quad (12)$$

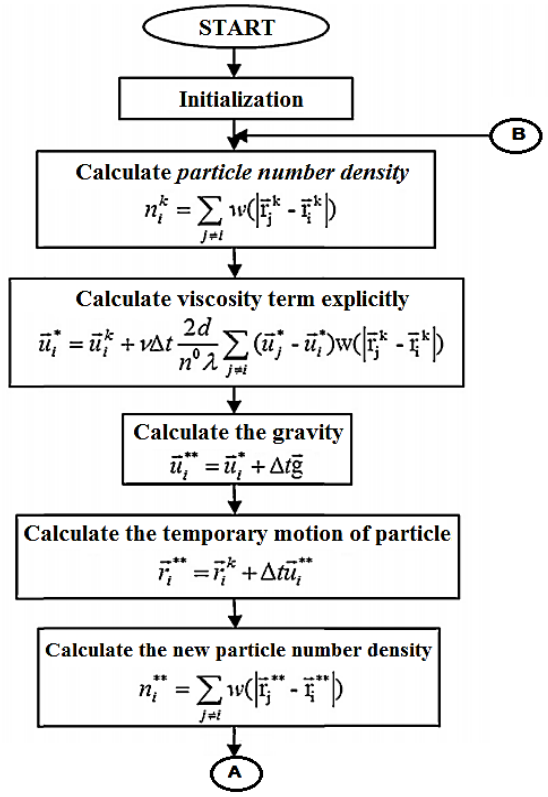

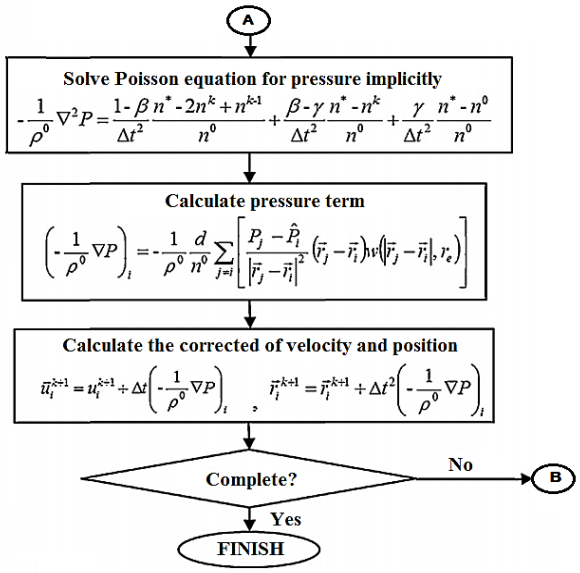

Fig. 3. Flowchart of the MPS method.

All process of calculations in this study are illustrated in the flowchart of the source-code as shown in Fig. 3. Calculations of first half were performed explicitly by using the finite difference method and calculations of second half were performed implicitly by using Crank-Nicholson method. In this study, the observed parameters are distance of the jump (x_1) and height of the jump (y_2) by varying reservoir level (H).

SIMULATION

To perform the simulation, the dimensions and geometric shape are shown in Fig. 4. The reservoir level (H) was set to 10 m, 18 m, and 32 m. The exhaust hole and the crested weir height are 1 m of height. The crested weir (green box) was placed at 55 m in front of the exhaust hole. The used particle size is 0.1 m. Using 18,174 particles for a height of 10 m, 23,934 particles for a height of 18 m, and 33,942 particles for a height of 32 m, a 30-second simulation was conducted. This design was adopted from the model outlined by López et al. [2]. The used liquid is fresh water which has a density of 1000 kg/m^3 and a kinematic viscosity of 1.004×10^{-6} m/s^2.

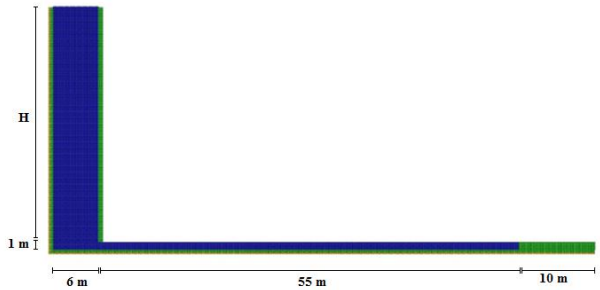

Fig. 4. Initial condition with the geometric.

RESULTS

1. Case A: Initial reservoir level of 10 m

At t = 1 s, a wave peak (y_2 = 3.38 m) appears in the region in front of the exhaust hole, as depicted in Fig. 5. In addition, at t = 2 s the wave height continues to increase (y_2 = 3.60 m), while at t = 5 s it begins to decrease (y_2 = 2.92 m). This decrease in wave height makes the hydraulic jump simpler to observe. At t = 5 s to t = 10 s, the height of the jump is between 2.92 m and 3.04 m. The water in the reservoir begins to drain after t = 11.5 s, at which point the height after the jump (y_2) decreases to 2.68 m.

The obtained results of this study are compared to those of López et al as shown in Table 1. Based on Fig. 5, it can be seen that the water surface height patterns are identical. In all other respects, the waveforms are nearly identical. In both of these experiments, the distance of the hydraulic jump was comparable. This demonstrates that the primary research conducted was excellent.

The process of pressure distribution is depicted in Fig. 6. At t = 1.85 s, a red zone can be observed in the region in front of the exhaust hole. Over time, the pressure distribution within the reservoir also decreases. After t = 3.85 s, there were no more red areas around the channel, with the exception of the reservoir. This indicates a pressure distribution below 50,000 Pa.

Table 1. The obtained results for H = 10 m.

t (s)	This study		Exp. [2]		SPH [2]	
	x_1 (m)	y_2 (m)	x_1 (m)	y_2 (m)	x_1 (m)	y_2 (m)
0.5	62.0	2.53				
1.0	64.4	3.38				
2.0	70.5	3.60				
3.0	77.3	3.01				
5.0	69.5	2.92	70.00	3.37	70.40	3.00
7.5	72.1	3.21				
10.0	75.9	3.04	82.00	3.90	80.00	3.82
11.5	76.3	2.68				
15.0	75.1	2.21	92.70	4.03	86.60	3.89

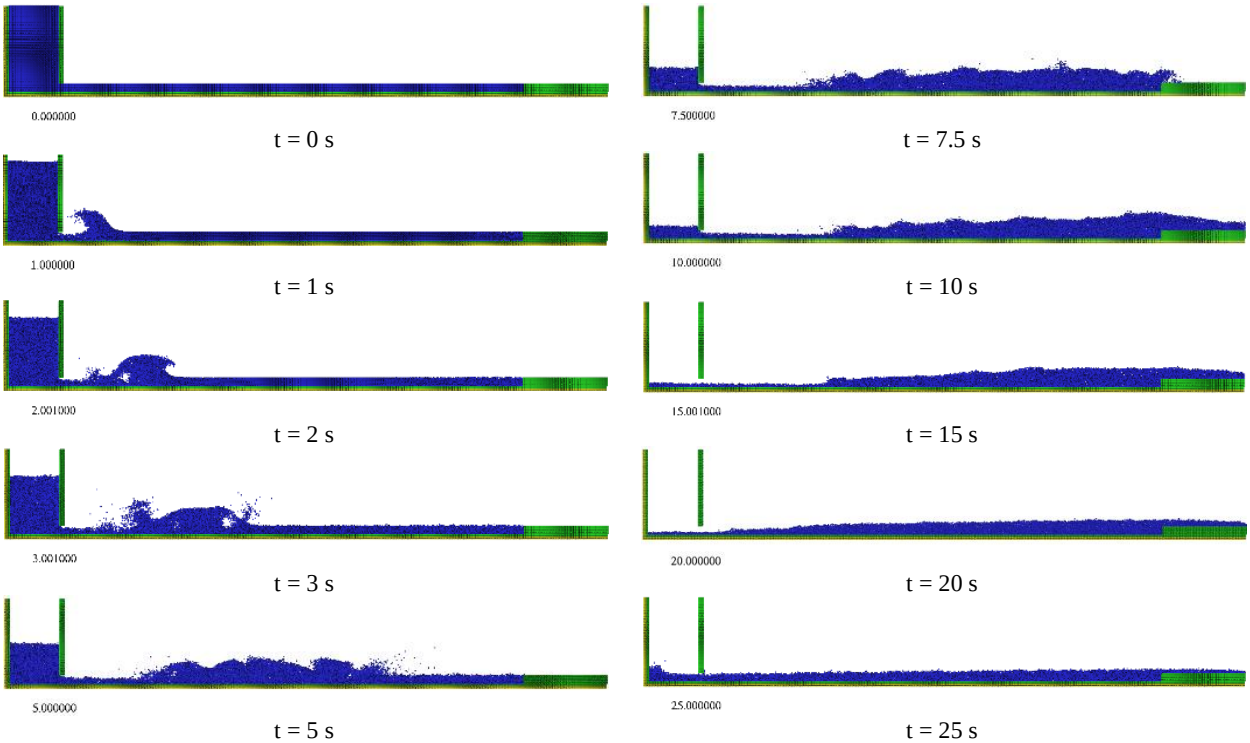

Fig. 5. Simulation process for H = 10 m.

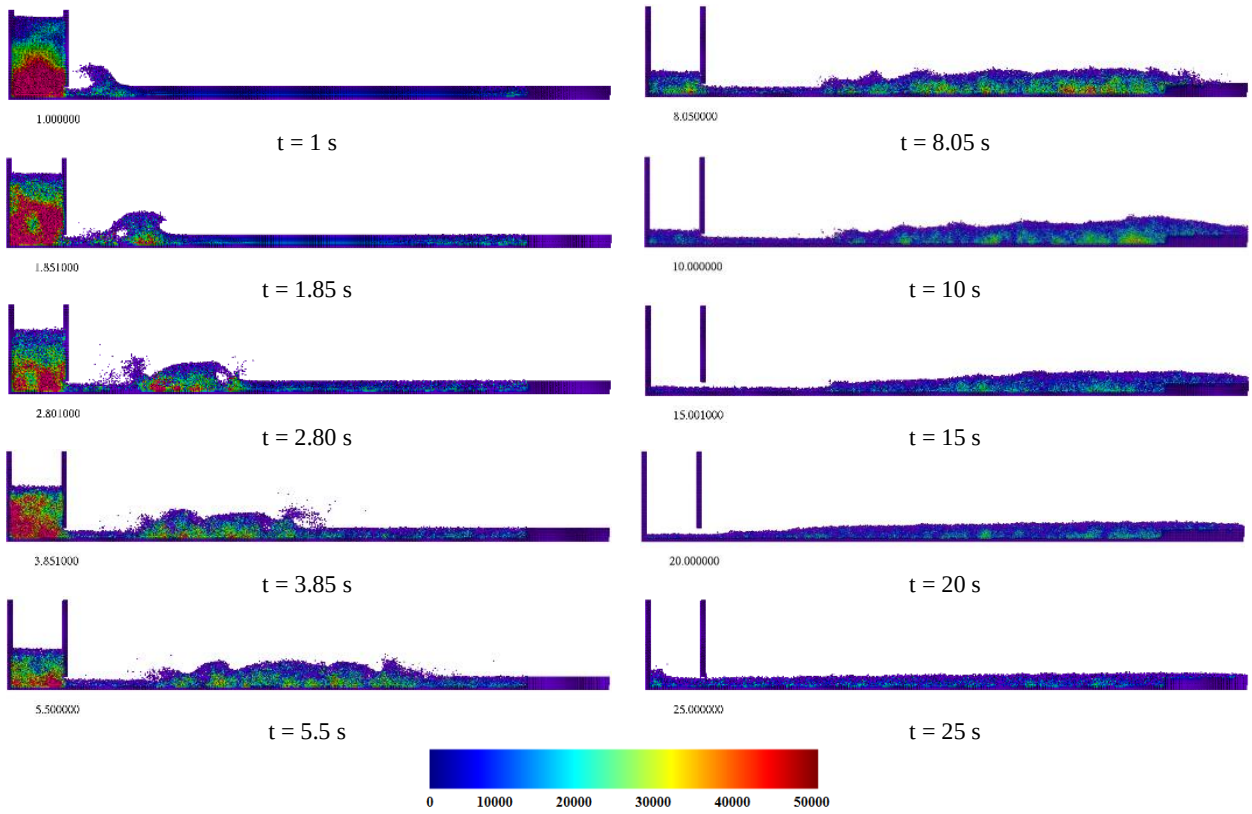

Fig. 6. Pressure distribution (in Pa unit) for H = 10 m.

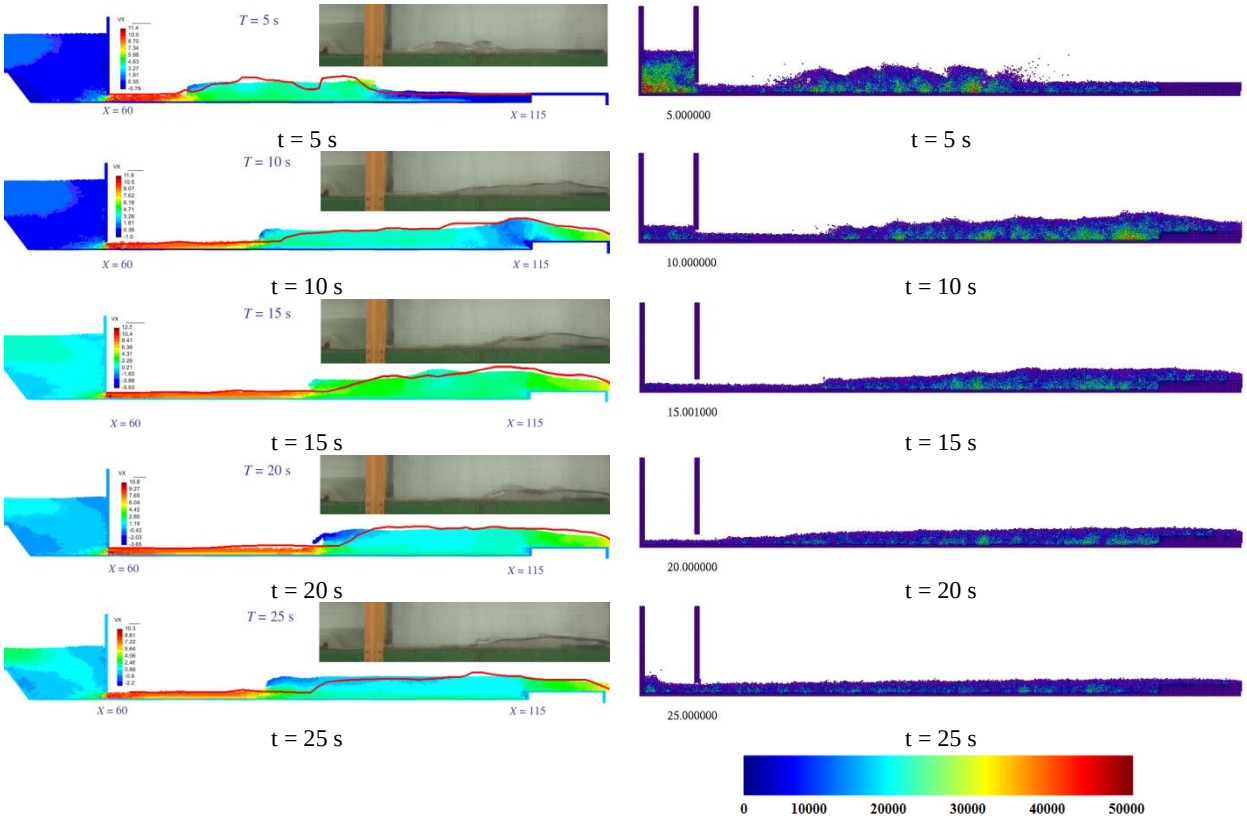

Fig. 7. Comparison results obtained by López et al. [2] and this study for H = 10 m.

2. Case B : Initial reservoir level of 18 m

Fig. 8 depicts the process of transporting water from the reservoir to the weir via a 55-meter-long channel. The water exits the reservoir through the exhaust hole and travels along the channel to the weir. At t = 0.5 s, the area in front of the exhaust hole (y_2 = 3.07 m) displays a wave peak, as depicted in Fig. 8. Until t = 2 s (y_2 = 5.18 m), the wave height continues to increase. The wave height begins to decrease at t = 3 s (y_2 = 4.56 m) and continues until t = 15.0 s (y_2 = 3.50 m). The water in the reservoir begins to drain after t = 15.5 s, at which point the height after the jump decreases to 2.90 m.

Fig. 9 depicts the distribution of pressure for an initial height of 18 meters. In contrast to the results obtained when the initial water height in the reservoir was 10 m, areas with pressures above 50,000 Pa were still detected until t = 10 s when the initial reservoir level was 18 m. After t = 15 s, there were no longer any red areas around the conduit or within the reservoir.

Fig. 10 compares the results of López et al. with those of this study. Based on Fig. 10, it is evident that the patterns of water level are identical. Additionally, the waveforms are comparable. The distance of the hydraulic jump is also comparable between the two studies, although it can be observed that the first jump distance obtained by López et al. is closer to the front of the exhaust hole than the results of this study as shown in Table 2. This discrepancy develops because of divergent methodologies, particularly in the initial reservoir configuration.

Table 2. The obtained results for H = 18 m.

t (s)	This study		Exp. [2]		SPH [2]	
	x_1 (m)	y_2 (m)	x_1 (m)	y_2 (m)	x_1 (m)	y_2 (m)
0.5	61.8	3.07				
1.0	65.0	4.67				
2.0	67.1	5.18				
3.0	72.9	4.56				
5.0	76.9	4.47	69.50	5.50	68.30	5.50
7.5	83.6	3.91				
10.0	94.4	4.82	79.40	6.30	76.40	5.60
15.0	92.8	3.50	83.60	5.70	81.00	5.50
15.5	91.9	2.90				

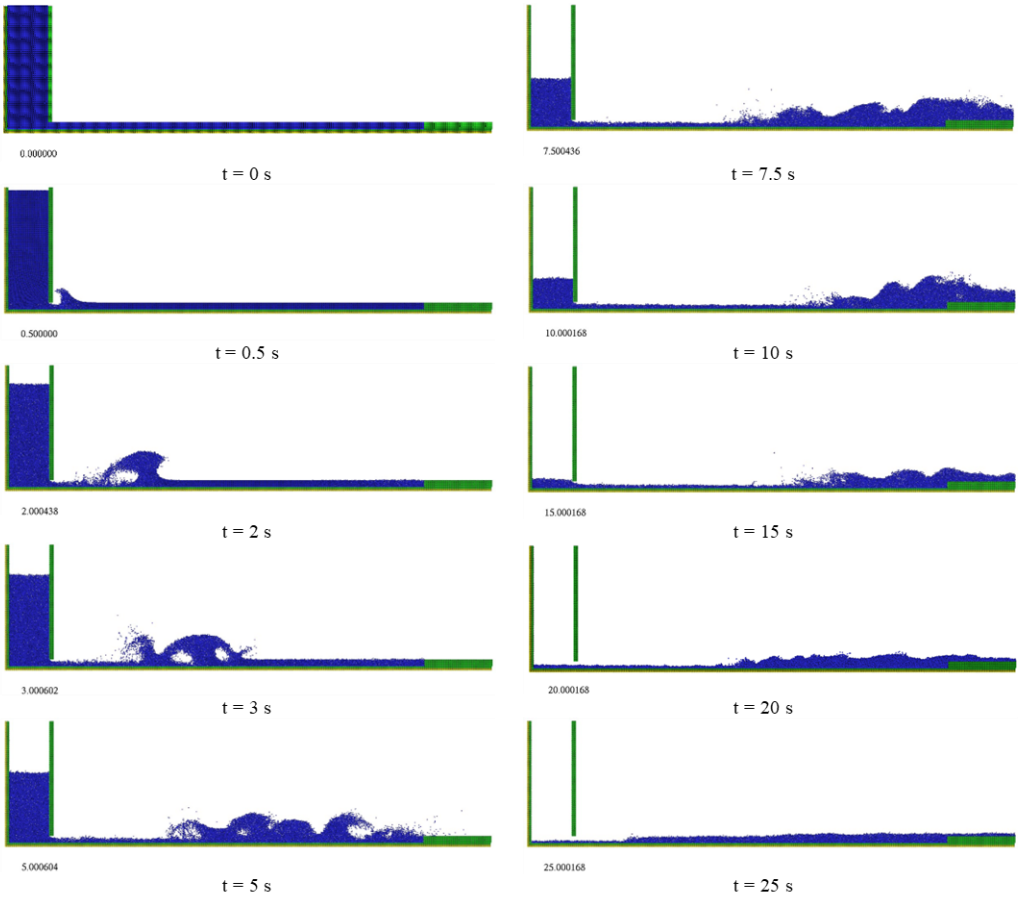

Fig. 8. Simulation process for H = 18 m.

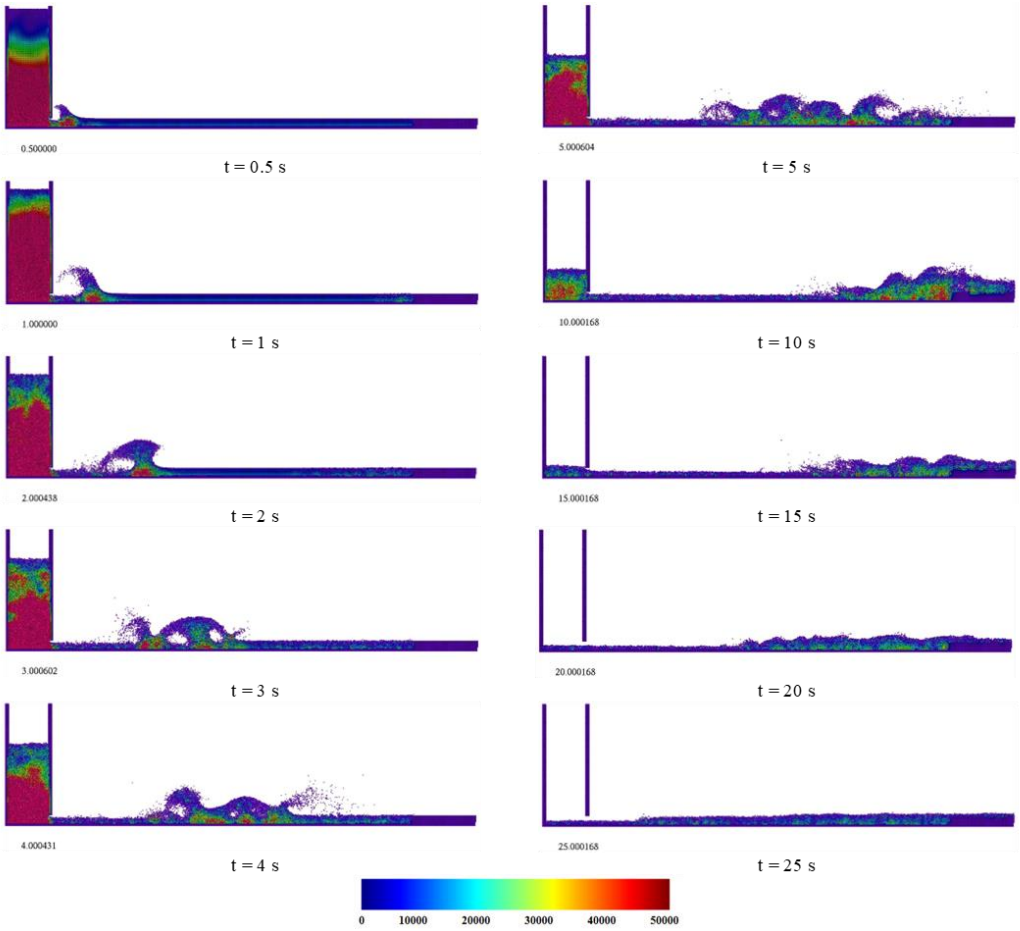

Fig. 9. Pressure distribution (in Pa unit) for H = 18 m.

3. Case C : Initial reservoir level of 32 m

Fig. 11 illustrates a simulation of the initial 32-meter of the reservoir level. At t = 0.5 s (y_2 = 2.98 m), it can be seen that there is a wave peak in the area in front of the exhaust hole. At t = 2 s, the wave height increases to 8.28 m and then begins to decrease until t = 20 s (y_2 = 15 m). Additionally, at t = 21.65 s, the water in the reservoir is entirely drained, and the height after the jump is 3.36 m.

The pressure distribution for an initial height of 32 m is depicted in Fig. 12. In contrast to the results when the initial reservoir level was 10 m and 18 m, in the case of a height of 32 m, there were still areas with pressures above 50,000 Pa until t = 20 s.

Table 3. The obtained results for H = 32 m.

t (s)	This study		Exp. [2]		SPH [2]	
	x_1 (m)	y_2 (m)	x_1 (m)	y_2 (m)	x_1 (m)	y_2 (m)
0.5	61.7	2.98				
1.0	67.6	5.58				
2.0	77.5	8.28				
3.0	73.8	7.50				
5.0	95.8	6.52	65.80	7.90	66.00	8.20
7.5	97.3	6.47				
10.0	100.7	6.39	77.50	8.20	76.00	8.00
15.0	95.6	5.53	81.00	7.50	70.50	8.20
20.0	92.9	4.15	79.40	6.60	60.00	7.60
21.65	91.3	3.36				

After t = 20 s, there were no red areas around the channel or inside the reservoir.

Fig. 13 presents a comparison between the obtained results of López et al. and those of this study, as illustrated in Table 3. The pattern of water level and the distance of the hydraulic jump from the front of the exhaust hole differs from the results obtained by López et al., as depicted in Fig. 13. This disparity arises from variations in the techniques, particularly in the initial layout of the reservoir. In general, however, the occurrence patterns of hydraulic jumps are still quite similar between this study and the reference.

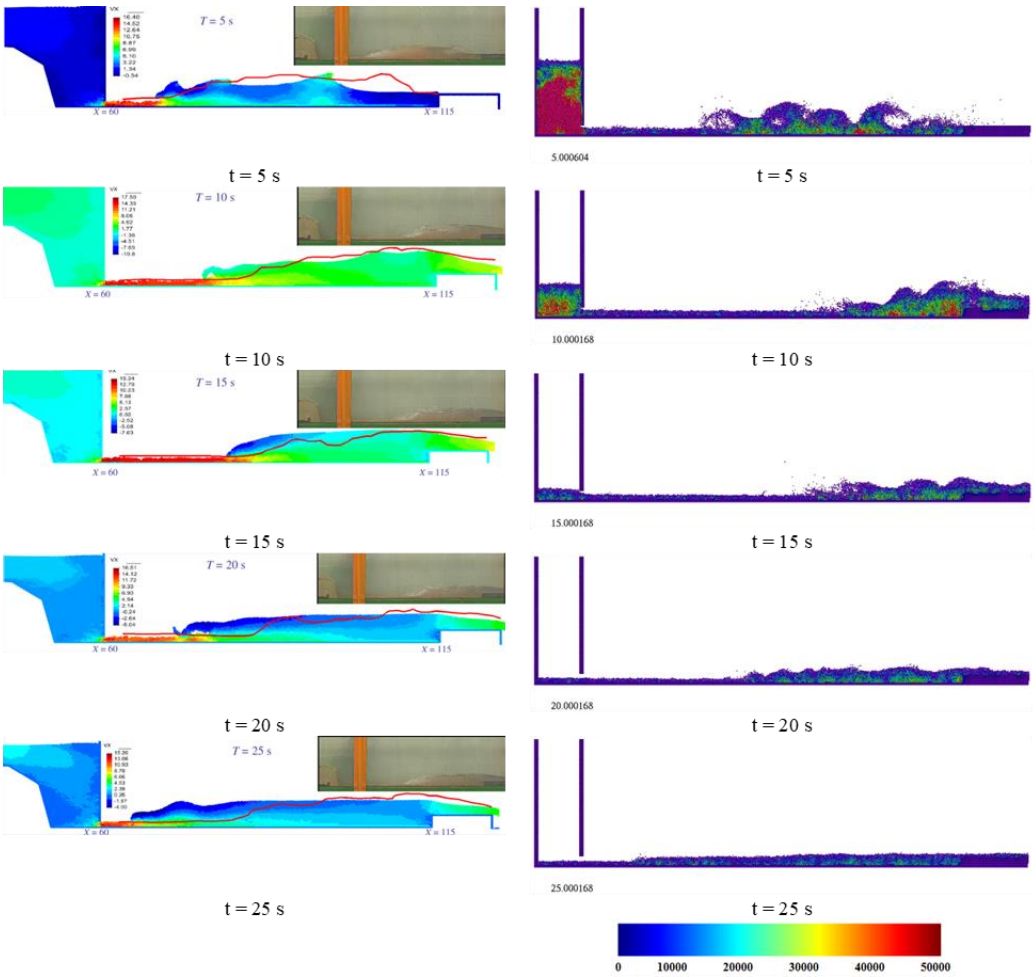

Fig. 10. Comparison results obtained by López et al. [2] and this study for H = 18 m.

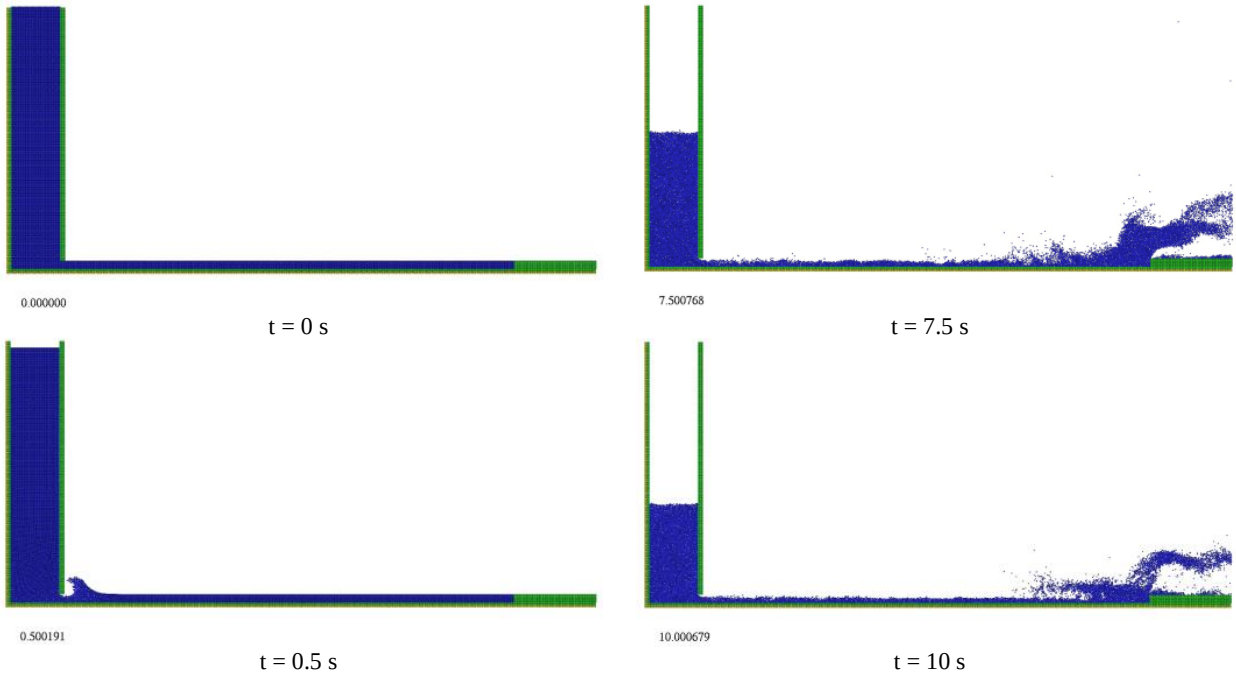

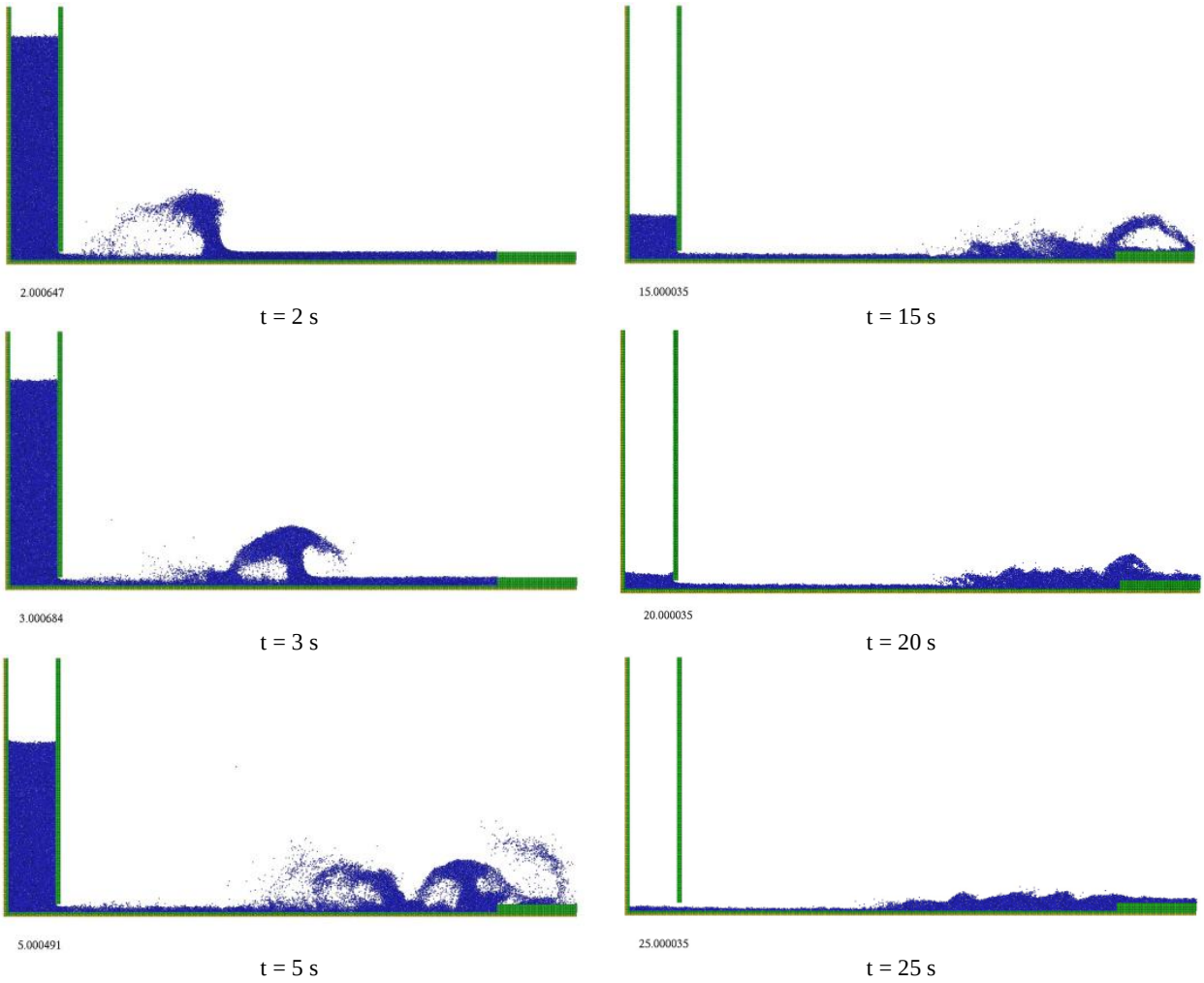

Fig. 11. Simulation process for H = 32 m.

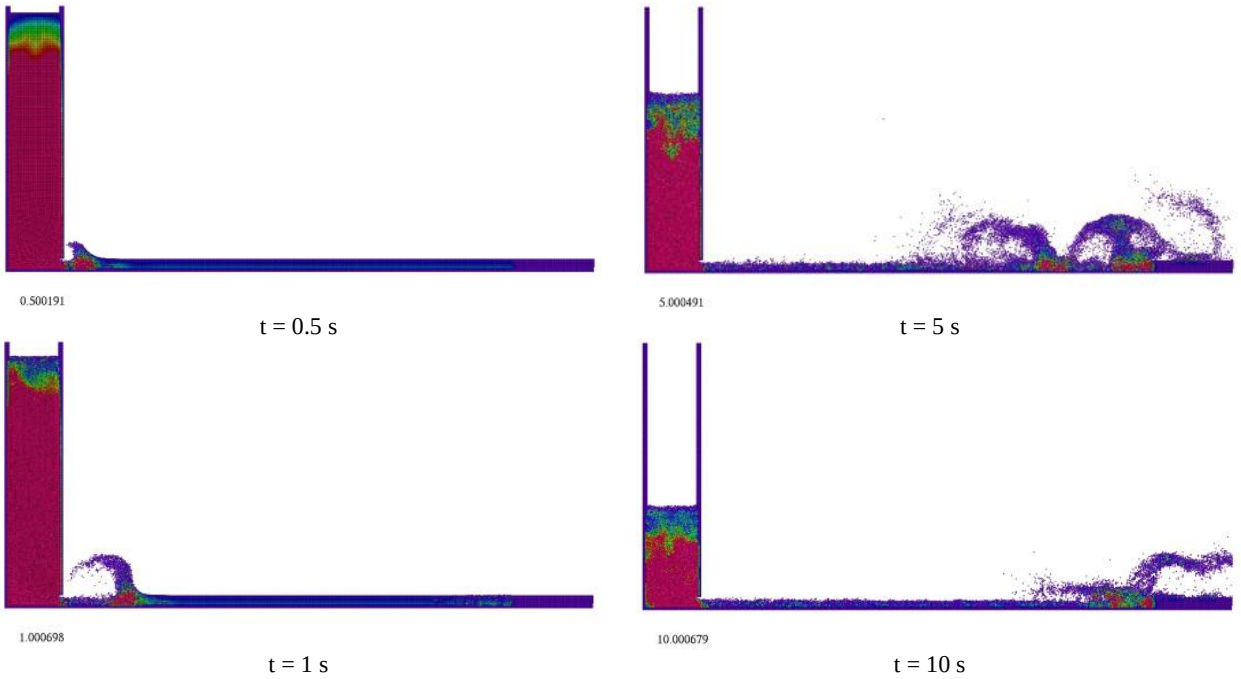

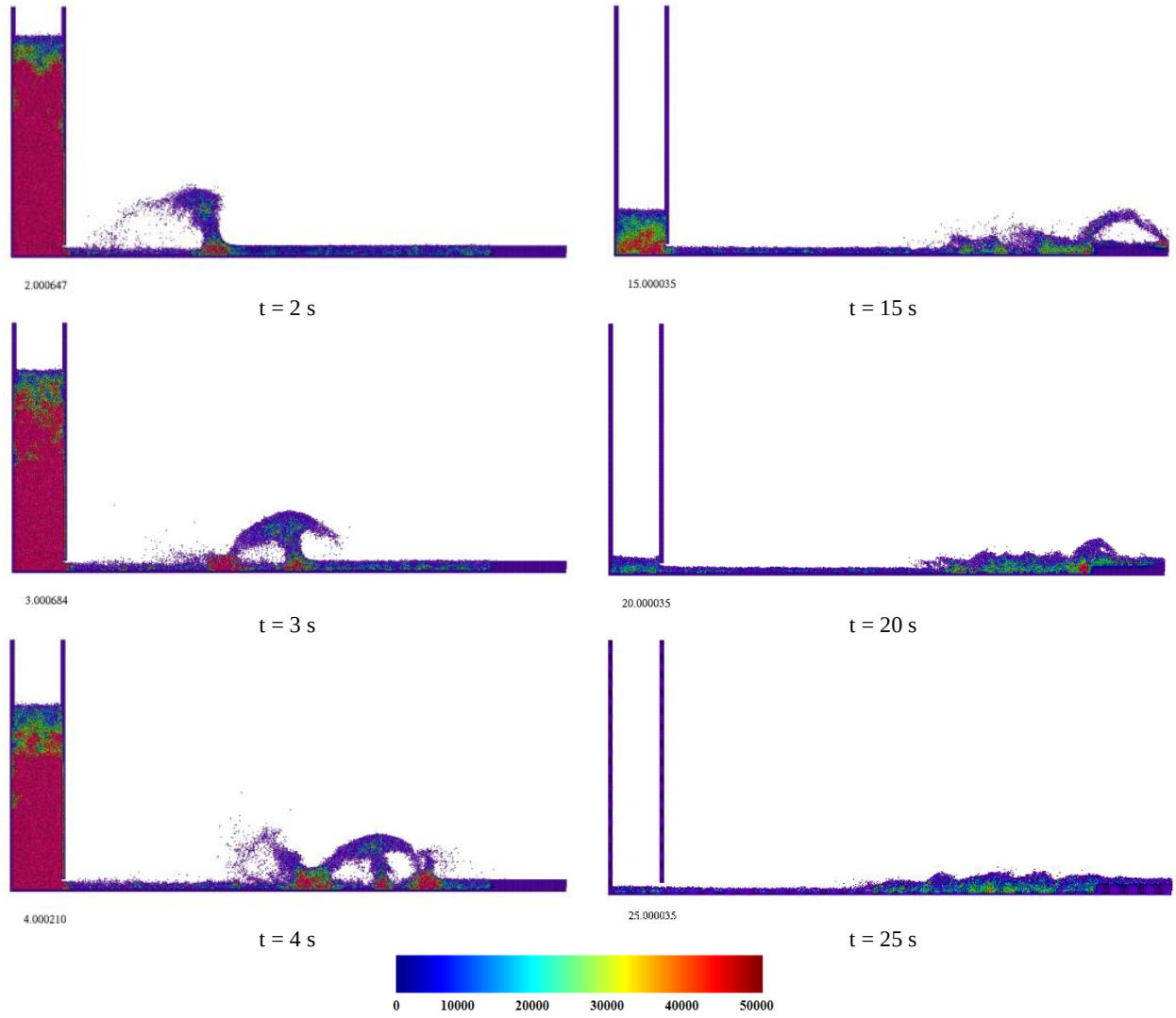

Fig. 12. Pressure distribution for H = 32 m.

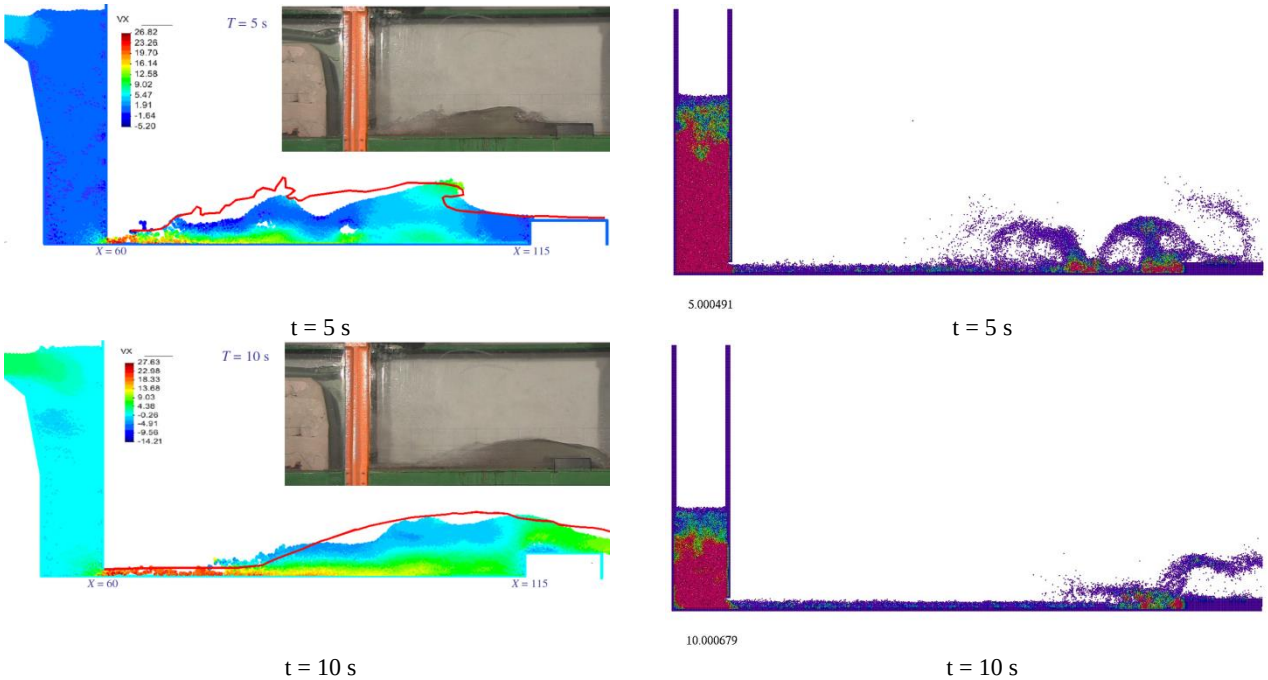

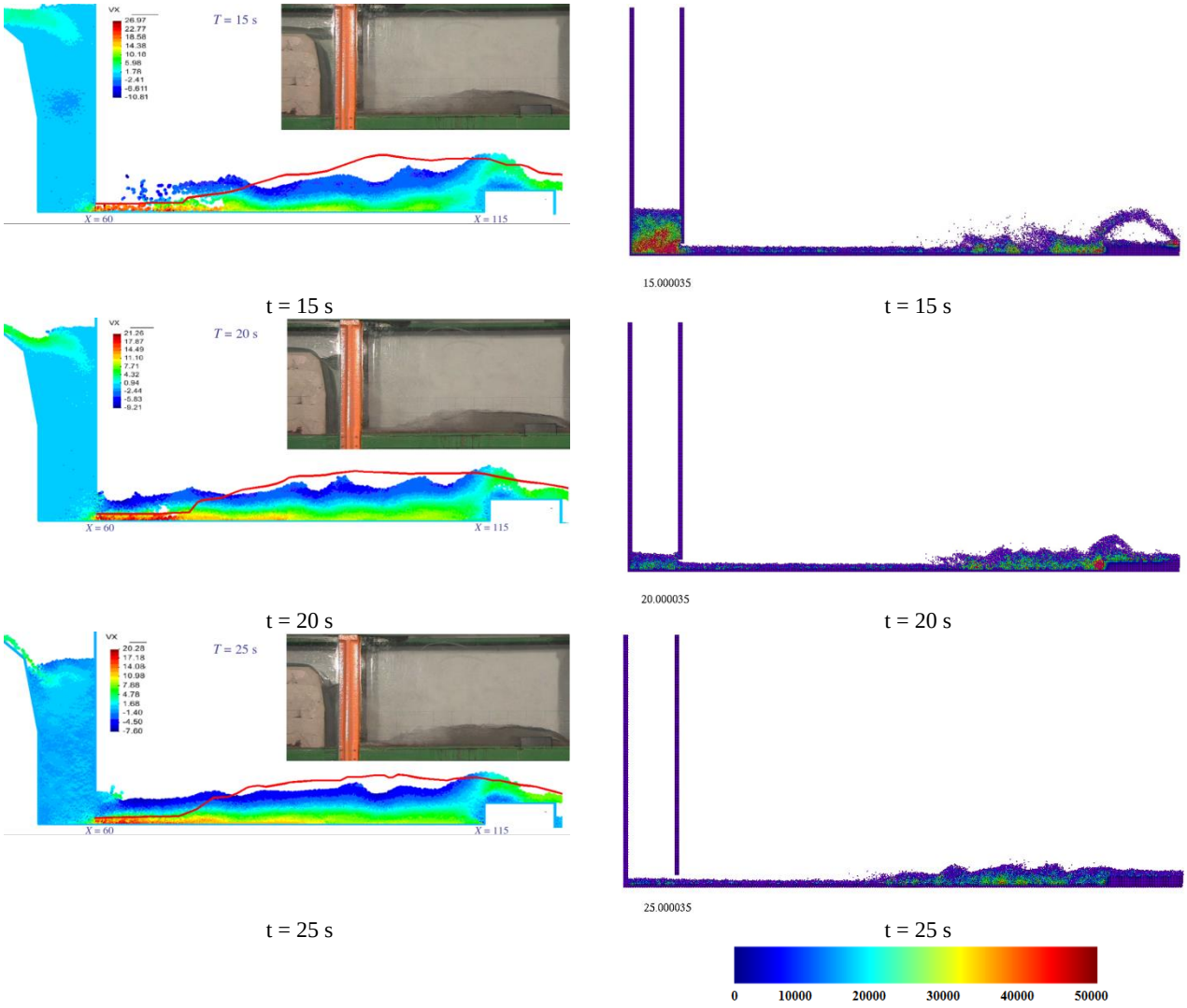

Fig. 13. Comparison results obtained by López et al. [2] and this study for H = 32 m.

DISCUSSION

In the first few seconds, as depicted in Fig. 5, Fig. 8, and Fig. 11, a splash wave appears in front of the exhaust hole. High hydrostatic pressure exerted on the particles from the reservoir forces them to migrate out of the exhaust hole, resulting in the formation of these waves. In addition, particulates in front of the exhaust hole are restrained by a weir with 55 meters (green area) from the front of exhaust hole. This causes particles from the reservoir to drive particles from outside the reservoir, resulting in waves/splashing.

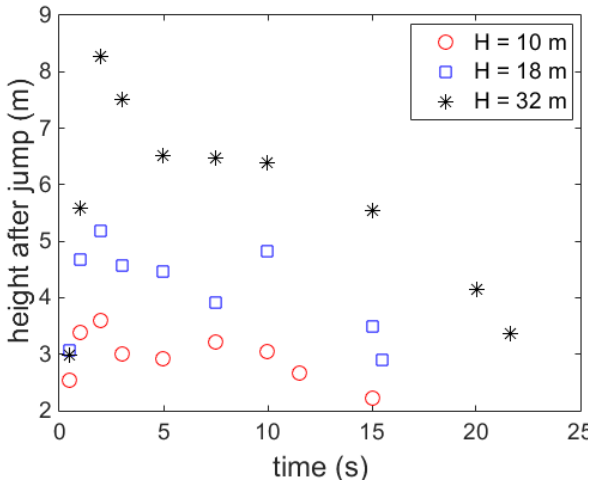

Fig. 14. Time vs. height after jump.

In addition, the water level in the reservoir impacts both the distance of the hydraulic jump from

the front of the exhaust hole (x_1) and the height after jump (y_2), as shown in Fig. 15. This is because the water level in the reservoir influences the speed of the water passing through the exhaust hole. The greater the reservoir level, the greater the water velocity through the exhaust hole, and consequently, the greater the hydraulic jump distance from the front of the exhaust hole (x_1).

When the waves/sparks that result from the collision of two types of particles with differing velocities have begun to diminish, the process of a hydraulic jump is readily observable. Particles that come from the reservoir with the greater speed collide with particles that were previously outside the hole and do not move. As a consequence, the faster particles push uphill and cause a hydraulic jump, resulting in a greater height after the jump than before it.

The obtained results of this study indicate that the reservoir level has an effect on the water surface height after the jump (y_2) as shown in Fig. 14. This is because the reservoir level influence the speed of the water passing through the exhaust hole. The higher the reservoir level, the greater the velocity of the water through the exhaust hole, and consequently the higher the height after the jump.

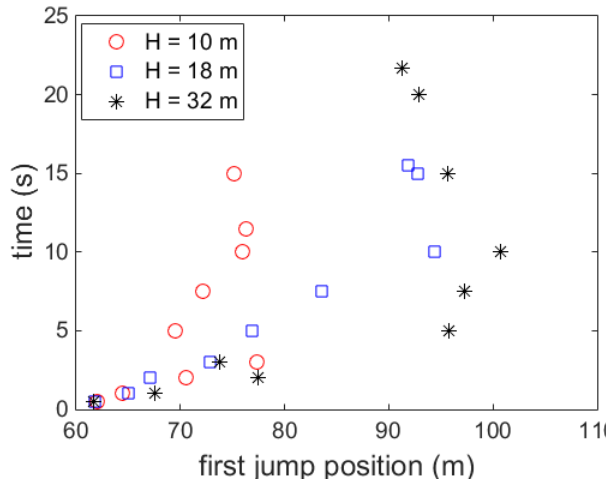

Fig. 15. First jump position vs. time.

From Figure 10, it can be seen that height after jump with the reservoir level of 32 m is highest among them. It means that the height after jump is equal to the reservoir level. From Figure 11, it can be seen that the first jump position from the front of the exhaust hole with the reservoir level of 10 m is shortest among them. It means that the first jump position is equal to the reservoir level.

CONCLUSION

A 2D simulation of the hydraulic jump procedure utilizing the reservoir-emptying procedure has been executed. Consistent with the obtained results of other researchers, the results of the simulation are quite favorable. From this study, it is obtained that the height of the reservoir after the jump is between 2.68 m and 3.60 m for an initial reservoir level of 10 m. For an initial reservoir level of 18 m, the height of the jump is between 2.90 and 5.18 m. The final height after the jump ranges from 2.98 m to 8.28 meters for an initial reservoir level of 32 m. Additionally, the maximum height after the jump is 3.6 m and the first jump position is 70.5 m when the initial height of the reservoir is 10 m. When the initial height of the reservoir is 18 m, the maximum height after the jump is 5.2 m and the first jump position is 67.1 m. When the initial height of reservoir is 32 m, the maximum height after jump is 8.2 m and the first jump position is 77.5 m. Based on the obtained results of this study, the higher the water level in the reservoir, the higher the water level after the jump. Moreover, the jump distance from the front of the exhaust hole increases as the reservoir level rises. Concerning the expansion of this study, additional research must be conducted to investigate this phenomenon in greater depth, particularly in terms of particle velocity during the hydraulic jump process.

ACKNOWLEDGMENT

This investigation is sponsored in its entirety by PPMI ITB 2022. The simulation source code is adopted from the research of Prof. Koshizuka, Prof. Sakai, and Dr. Shibata.

REFERENCES

[1] K. Laishram, P. A. Kumar, and T. T. Devi, “Effect of channel slope and roughness on hydraulic jump in open channel flow,” *IOP Conf. Ser. Earth Environ. Sci.*, vol. 958, p. 012014, 2022, doi: 10.1088/1755-1315/958/1/012014.

[2] D. López, R. Marivela, and L. Garrote, “Smoothed particle hydrodynamics model applied to hydraulic structures: a hydraulic jump test case,” *J. Hydraul. Res.*, vol. 48, pp. 142–158, 2010, doi: 10.3826/jhr.2010.0015.

[3] C. Cheng, Y. Tai, and Y. Jin, “Particle Image Velocity Measurement and Mesh-Free Method Modeling Study of Forced Hydraulic Jumps,” *J. Hydraul. Eng.*, vol. 143, no. 9, p. 04017028, 2017, doi: 10.1061/(ASCE)HY.1943-7900.0001325.

[4] D. Bonn, A. Andersen, and T. Bohr, "Hydraulic jumps in a channel," *J. Fluid Mech.*, vol. 618, pp. 71–87, 2009, doi: 10.1017/S0022112008004540.

[5] S. Koshizuka and Y. Oka, "Moving-Particle Semi-Implicit Method for Fragmentation of Incompressible Fluid," *Nucl. Sci. Eng.*, vol. 123, pp. 421–434, 1996, doi: 10.13182/NSE96-A24205.

[6] S. Koshizuka, A. Nobe, and Y. Oka, "Numerical analysis of breaking waves using the Moving Particle Semi-Implicit method," *Int. J. Numer. Methods Fluids*, vol. 26, pp. 751–769, 1998.

[7] S. Koshizuka and Y. Oka, "Mowing Particle Semi-Implicit Method: Fully Lagrangian Analysis of Incompressible Flows," in *European Congress on Computational Methods in Applied Sciences and Engineering*, 2000, pp. 1–16.

[8] S. Koshizuka, S. Kazuya, K. Masahiro, and M. Takuya, *Moving Particle Semi-implicit Method - A Meshfree Particle Method for Fluid Dynamics*. Academic Press, 2018.

[9] G. Li, Y. Oka, M. Furuya, and M. Kondo, "Experiments and MPS analysis of stratification behavior of two immiscible fluids," *Nucl. Eng. Des.*, vol. 265, pp. 210–221, 2013, doi: 10.1016/j.nucengdes.2013.09.006.

[10] Y. Yulianto, A. N. Hidayati, A. P. A. Mustari, M. Ilham, and S. Pramuditya, "Moving Particle Semi-implicit (MPS) Utilization in Analyzing the Stratification Behavior of Immiscible Liquid," *IOP Conf. Ser. Mater. Sci. Eng.*, vol. 407, p. 012189, 2018, doi: 10.1088/1757-899X/407/1/012189.

[11] Y. Yulianto, A. P. A. Mustari, and A. Baliana, "The stratification behavior of reactor materials in the framework of Moving Particle Semi-Implicit," *Indones. J. Nucl. Sci. Technol.*, vol. 02, no. 02, pp. 59–71, 2021.

[12] Y. Yulianto, A. P. A. Mustari, and A. Baliana, "The Simulation of the Stratification Process of Some Liquid Salts by Using the Moving Particle Semi-Implicit Method," *J. Phys. Conf. Ser.*, vol. 2243, p. 012065, 2022, doi: 10.1088/1742-6596/2243/1/012065.

[13] M. Ilham, Y. Yulianto, and A. P. A. Mustari, "Simulation on Relocation of Non-Compressed Fluid Flow using Moving Particle Semi-Implicit (MPS) Method," *IOP Conf. Ser. Mater. Sci. Eng.*, vol. 407, p. 012100, 2018, doi: 10.1088/1757-899X/407/1/012100.

[14] Y. Yulianto, A. P. A. Mustari, M. Ilham, A. N. Hidayati, and S. Hatmanti, "Moving Particle Semi-implicit Method in Simulating Water-Oil Penetration," *Indones. J. Phys.*, vol. 30, no. 2, pp. 25–33, 2019.

[15] Y. Yulianto and A. P. A. Mustari, "Numerical Study on Relocation Process of Al, Fe, and Pb by Using the Moving Particle Semi-Implicit Method During Severe Accident of Reactor," *Int. J. Technol.*, vol. 14, no. 4, pp. 800–810, 2023, doi: 10.14716/ijtech.v14i4.5240.

[16] A. P. A. Mustari, Y. Oka, M. Furuya, W. Takeo, and R. Chen, "3D simulation of eutectic interaction of Pb-Sn system using Moving Particle Semi-implicit (MPS) method," *Ann. Nucl. Energy*, vol. 81, pp. 26–33, 2015, doi: 10.1016/j.anucene.2015.03.031.

[17] A. P. A. Mustari and Y. Oka, "Molten uranium eutectic interaction on iron-alloy by MPS method," *Nucl. Eng. Des.*, vol. 278, pp. 387–394, 2014, doi: 10.1016/j.nucengdes.2014.07.028.